Inorganic Chemistry

Article

pubs.acs.org/IC

# Synthesis, Structure, Photophysics, and a DFT Study of Phosphorescent C*N^N- and C^N^N-Coordinated Platinum Complexes

Caleb F. Harris,[†,§] Dileep A. K. Vezzu,[†] Libero Bartolotti,[†] Paul D. Boyle,[‡,∥] and Shouquan Huo*[,†]

[†]Department of Chemistry, East Carolina University, Greenville, North Carolina 27858, United States

[‡]Department of Chemistry, North Carolina State University, Raleigh, North Carolina 27695, United States

Supporting Information

**ABSTRACT:** The reaction of *N*,*N*-diphenyl-2,2′-bipyridin-6-amine (**L1**) and *N*,*N*-diphenyl-6-(1*H*-pyrazol-1-yl)pyridin-2-amine (**L2**) with $K_2PtCl_4$ produced C*N^N-coordinated cycloplatinated compounds with a five−six fused metallacycle **1a** and **2a**, respectively, which were then converted into their phenylacetylide derivatives **1b** and **2b**, respectively. Similar reactions starting from 2-phenyl-6-(1*H*-pyrazol-1-yl)pyridine (**L3**) produced C^N^N-coordinated platinum complexes **3a** and **3b** with a five−five-fused metallacycle. The structures of **1a**, **1b**, **2b**, **3a**, and **3b** were determined by X-ray crystallography. The C*N^N-coordinated platinum complexes are closer to a square geometry, whereas the C^N^N-coordinated complexes display a nearly perfect planar geometry. The $\pi\cdots\pi$ interactions were revealed in the crystal packing for **1a**, **2b**, and **3a** with a $\pi\cdots\pi$ contact of 3.450, 3.422, and 3.414 Å, respectively. Two conformers were revealed in the crystal structure of **2b**, one with the phenyl ring of the phenylacetylide being approximately parallel with the coordination plane and the other with the phenyl ring being approximately perpendicular to the coordination plane. Both **1a** and **1b** are weakly emissive in the red region. Complexes **2a** and **3a** are also weakly emissive, but their acetylide derivatives **2b** and **3b** emitted strongly green light at room temperature with quantum yields of 43 and 62%, respectively. DFT/TDDFT calculations were performed to elucidate the nature of their electronic transitions. The calculations suggested that lowest singlet and triplet excited states are characteristic of a mixed state involving one or more charge-transfer transitions such as ILCT, MLCT, and LLCT.

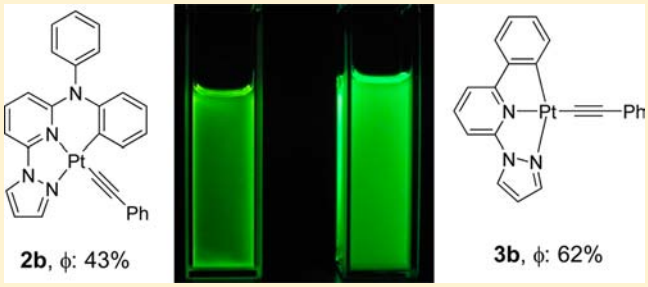


## INTRODUCTION

Phosphorescent materials based on cyclometalated platinum complexes have recently attracted a great deal of attention because of their potential in chemical,[1] biological,[2] and optoelectronic applications, particularly as phosphorescent emitter in OLED (organic light-emitting diode) devices.[3] Ligand design remains a main tool of manipulating the photophysical properties, especially the phosphorescence efficiency of the complexes for those applications. Recently, we have developed a series of highly efficient phosphorescent cyclometalated platinum complexes with a fused five−six-membered metallacycle, which include tridentate C^N*N-[4] and N^C*N-coordinated[5] platinum complexes and tetradentate C^N*N^C-,[6] N^C*C^N-,[6] and C^C*N^N-coordinated[7] platinum complexes, where X^Y and X*Y (X, Y = C, or N) represents a bidentate coordination to the metal center through a five-membered metallacycle and through a six-membered metallacycle, respectively. The ligand design involves the use of an amine linker to extend the more conventional five-membered metallacycle into a six-membered ring. These complexes have displayed generally high photoluminescence quantum yields, and some of them are among the brightest phosphorescent emitters. Other examples of phosphorescent cyclometalated platinum complexes with a fused five−six metallacycle have also been reported.[8] In the tridentate C^N*N-[4] and N^C*N-coordinated[5] platinum complexes, the use of the amine linker, specifically the aniline linker, effectively prevented the formation of excimers or aggregates that could cause the self-quenching of the emission. This can be reasoned by the perpendicular orientation of the *N*-phenyl ring with respect to the coordination plane, which makes the intermolecular interaction more difficult. The absence of the self-quenching can be advantageous when the emitter is used as a triplet dopant in an OLED device where the emitter is doped into the host at relatively high concentration.[8c] The photoluminescence quantum efficiencies of the N^C*N-coordinated[5] platinum complexes are comparable to those of highly emissive N^C^N-coordinated platinum complexes,[9] while C^N*N-coordinated[4] platinum complexes displayed higher efficiency than those of more conventional C^N^N-coordinated[10] complexes. One explanation for the better emission efficiency

**Received:** March 25, 2013
**Published:** October 2, 2013

   dx.doi.org/10.1021/ic400732g | *Inorg. Chem.* 2013, 52, 11711−11722

**Chart 1. Schematic Representation of N^C^N, C^N^N, N^C*N, C^N*N, and C*N^N-Coordinated Platinum Complexes**

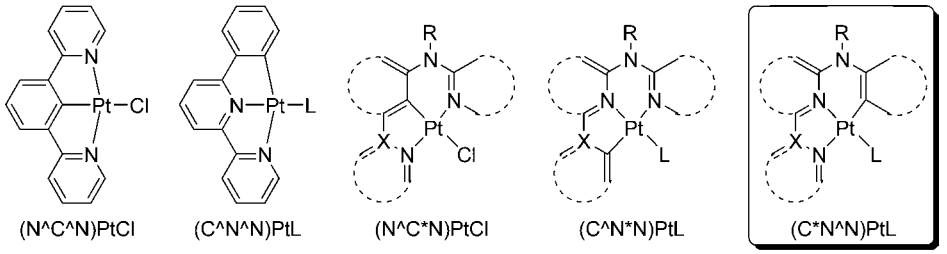


X= carbon or nitrogen, L = mono anionic ligand

**Scheme 1. Synthesis of the Ligands and the Complexes**

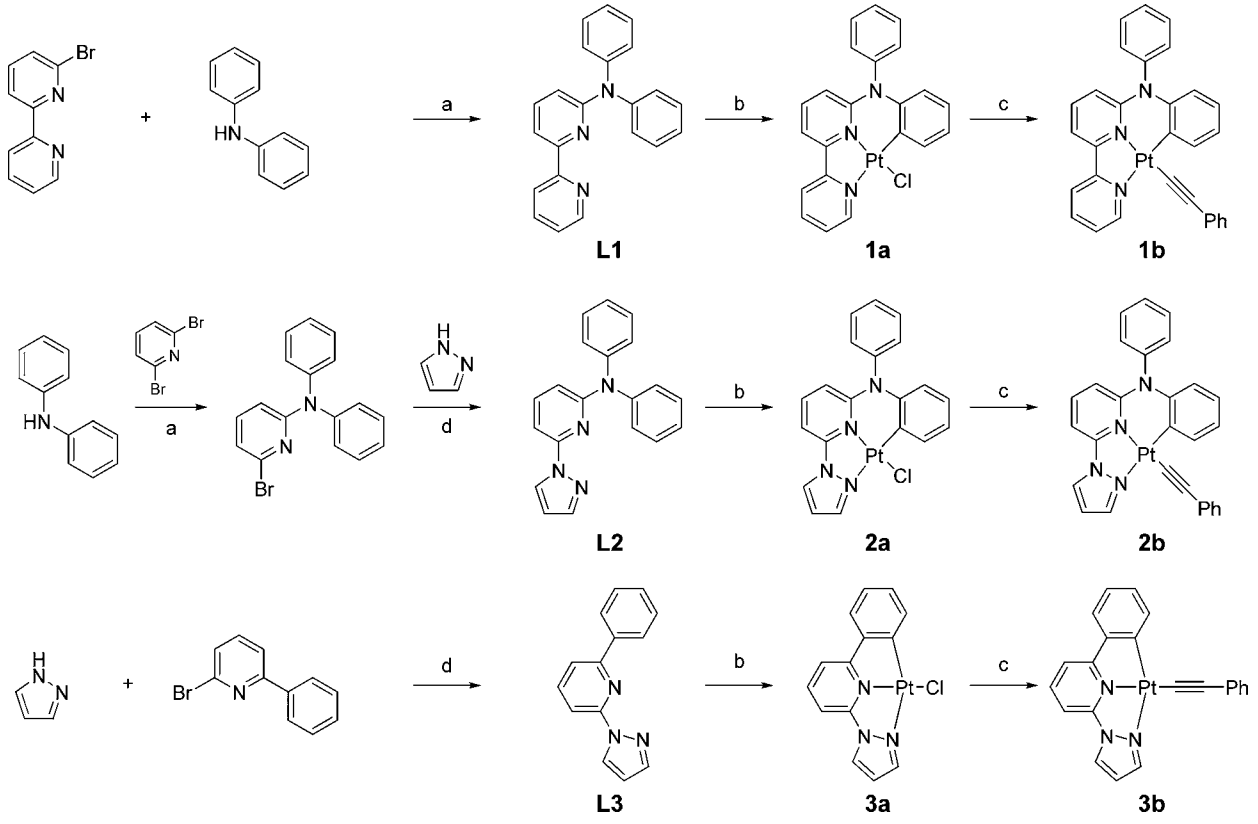


[a]Reagents and conditions: (a) $Pd(dba)_2$ (4%), DPPF (4%), NaO$^t$Bu (1.2 equiv), toluene, reflux; (b) $K_2PtCl_4$ (1 equiv), AcOH, reflux; (c) phenylacetylene, CuI, triethylamine, dichloromethane, room temperature; (d) CuI (10%), *trans-N,N′*-dimethylcyclohexanediamine (25%), $K_2CO_3$ (2.1 equiv), toluene, reflux.

is based on the geometrical change of the coordination from a fused five−five-membered metallacycle to a less strained five−six-membered ring; as a result, the square geometry for a platinum(II) complexes could be achieved through the increase of the biting angle from 160° in the C^N^N and N^C^N-coordinated complexes to greater than 170° in the C^N*N and N^C*N-coordinated platinum complexes. Such explanation has been proposed for other complexes particularly for the complexes with a fused six-six-membered metallacycle.[11] More recently, the adverse effect of a geometrical change from five−five-membered to six-six-membered ring was reported on the platinum complexes.[11a]

In order to substantiate the effect of the geometry change from five−five to five−six-membered metallacycle on the photophysical properties, it is necessary to consider all possible variations of coordination patterns of cyclometalated platinum complexes that form a five-six-membered metallacycle through coordinating to one carbon and two nitrogen coordinating atoms, namely C^N*N, N^C*N, and C*N^N-coordinated complexes as shown in Chart 1. Herein we report the synthesis, structure, and photophysical properties of C*N^N-coordinated platinum complexes, which are also compared with the corresponding C^N^-coordinated complexes.

## RESULTS AND DISCUSSION

**Synthesis.** Synthesis of the ligands and complexes is shown in Scheme 1. **L1** was prepared by the palladium-catalyzed C−N cross-coupling reaction[12] of diphenylamine with 6-bromo-2,2′-bipyridine in 89% yield. Complexation of **L1** with $K_2PtCl_4$ in acetic acid under reflux gave the complex **1a** in 74% yield, which was converted to **1b** in 95% yield by reacting with phenylacetylene in the presence of copper iodide and triethylamine. Ligand **L2** was prepared by sequential


dx.doi.org/10.1021/ic400732g | Inorg. Chem. 2013, 52, 11711−11722

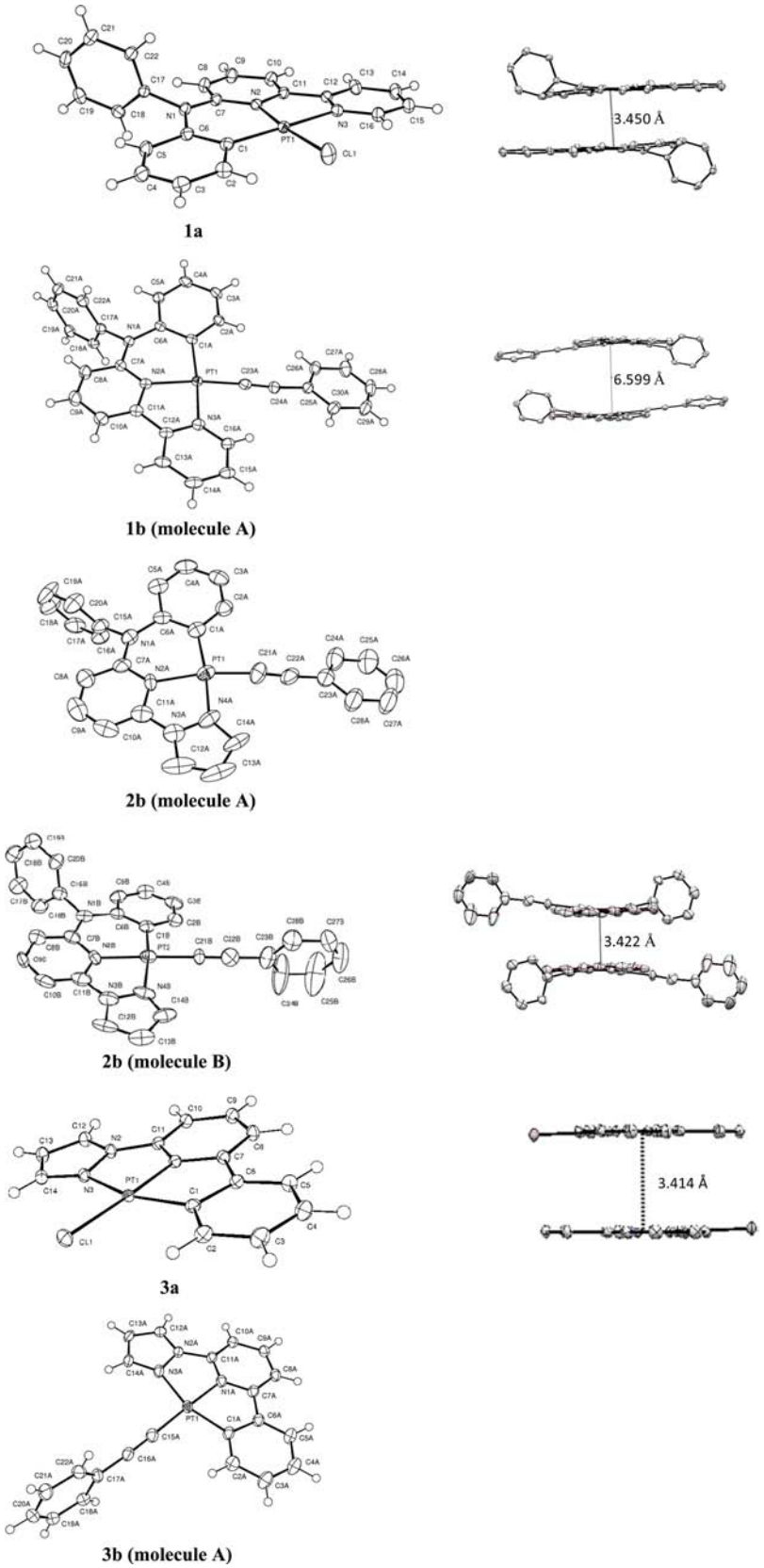


**Figure 1.** Perspective drawing of **1a** and **1b** (molecule A), **2b** (molecules A and B), and **3a** and **3b** (molecule A). Ellipsoids are at the 50% probability level. The $\pi\cdots\pi$ contacting distances between two molecules in the crystal packing are shown on the right for **1a**, **1b**, **2b**, and **3a**. There was no $\pi\cdots\pi$ interaction in the crystal packing of **3b**.

palladium-[12] and copper-catalyzed[13] C−N bond formation reactions. The preparation of ligand **L3** was achieved by the copper-catalyzed cross coupling[13] of 2-bromo-6-phenylpyridine with pyrazole. Complexes **2a**, **2b**, **3a**, and **3b** were prepared in


dx.doi.org/10.1021/ic400732g | *Inorg. Chem.* 2013, 52, 11711−11722

Table 1. Selected Bond Lengths (Å) and Angles (deg) for 1a, 1b, 2b, 3a, and 3b

| complex 1a | | complex 1b | | complex 2b | |
|---|---|---|---|---|---|
| Pt(1)−C(1) | 1.996(2) | Pt(1)−C(1A) | 1.988(3) | Pt(1)−C(1A) | 1.976(9) |
| Pt(1)−N(2) | 1.9993(19) | Pt(1)−N(2A) | 2.040(2) | Pt(1)−N(2A) | 2.043(7) |
| Pt(1)−N(3) | 2.091(2) | Pt(1)−-N(3A) | 2.071(2) | Pt(1)−N(4A) | 2.078(8) |
| Pt(1)−Cl(1) | 2.3140(6) | Pt(1)−C(23A) | 1.950(3) | Pt(1)−C(21A) | 1.946(11) |
| N(1)−C(7) | 1.377(3) | N(1A)−C(7A) | 1.381(3) | N(1A)−C(7A) | 1.393(12) |
| N(1)−C(6) | 1.429(3) | N(1A)−C(6A) | 1.442(3) | N(1A)−C(6A) | 1.451(11) |
| N(1)−C(17) | 1.451(3) | N(1A)−C(17A) | 1.456(3) | N(1A)−C(15A) | 1.459(11) |
| N(2)−Pt(1)−Cl(1) | 171.97(6) | C(23A)−Pt(1)−N(2A) | 173.64(10) | C(21A)−Pt(1)−N(2A) | 170.7(4) |
| C(1)−Pt(1)−N(3) | 174.85(9) | C(1A)−Pt(1)−N(3A) | 172.27(10) | C(1A)−Pt(1)−N(4A) | 171.4(3) |
| N(2)−Pt(1)−N(3) | 81.47(8) | C(1A)−Pt(1)−N(2A) | 93.67(10) | C(1A)−Pt(1)−N(2A) | 93.6(3) |
| C(1)−Pt(1)−Cl(1) | 94.26(7) | C(23A)−Pt(1)−N(3A) | 93.99(10) | C(21A)−Pt(1)−N(4A) | 93.3(4) |
| C(1)−Pt(1)−N(2) | 93.74(9) | C(23A)−Pt(1)−C(1A) | 92.06(11) | C(21A)−Pt(1)−C(1A) | 93.9(4) |
| N(3)−Pt(1)−Cl(1) | 90.51(6) | N(2A)−Pt(1)−N(3A) | 80.53(9) | N(2A)−Pt(1)−N(4A) | 79.7(3) |
| complex 3a | | complex 3b | | | |
| Pt(1)−C(1) | 1.989(2) | Pt(1)−C(1A) | 1.985(9) | | |
| Pt(1)−N(1) | 1.9539(15) | Pt(1)−N(1A) | 1.985(8) | | |
| Pt(1)−N(3) | 2.0986(18) | Pt(1)−N(3A) | 2.098(8) | | |
| Pt(1)−Cl(1) | 2.3101(9) | Pt(1)−C15(A) | 1.950(10) | | |
| C(1)−Pt(1)−N(3) | 160.86(6) | C(1A)−Pt(1)−N(3A) | 159.8(3) | | |
| N(1)−Pt(1)−Cl(1) | 177.76(4) | C(15A)−Pt(1)−N(1A) | 175.7(3) | | |
| N(1)−Pt(1)−N(3) | 79.13(5) | N(1A)−Pt(1)−N(3A) | 78.0(3) | | |
| N(1)−Pt(1)−C(1) | 81.73(6) | N(1A)−Pt(1)−C(1A) | 81.8(4) | | |
| C(1)−Pt(1)−Cl(1) | 99.92(5) | C(15A)−Pt(1)−C(1A) | 98.3(4) | | |
| N(3)−Pt(1)−Cl(1) | 99.22(4) | C(15A)−Pt(1)−N(3A) | 101.8(3) | | |

similar ways to those described for **1a** and **1b**, respectively. All ligands and complexes have been characterized by proton and carbon-13 NMR spectroscopy and satisfactory elemental analysis.

**X-ray Crystal Structures.** The molecular structures of the complexes **1a**, **1b**, **2b**, **3a**, and **3b** were determined by X-ray crystallography. The structures are shown in Figure 1. The crystal data and structure refinement details are provided in the Supporting Information (Table S1), and selected bond lengths and angles are listed in Table 1. The lengths of the Pt−C and Pt−N bonds are comparable to those found in other similar cyclometalated platinum complexes. The Pt−C (acetylide) bonds in **1b** (1.950(3) Å), **2b** (1.946(11) Å), and **3b** (1.950(10) Å) are considerably shorter than the Pt−C (aryl) bonds (1.976(9)−1.988(3) Å). Generally, the strength of bonds formed between platinum and different types of carbons increases in the order of $sp^3$, $sp^2$, and sp carbons, which is also observed in our recent study of cyclometalated platinum complexes.[4,14] The length of the Pt−N bonds varies with their environments. In **1a** and **3a**, the Pt−N bond that is *trans* to a Pt−C bond is significantly longer than the other Pt−N bond, indicating a strong structural *trans* effect[15] induced by the carbon donor. In **1b**, as the chloride ligand is replaced with an acetylide, and the Pt−N bond *trans* to the *sp* carbon of the acetylide becomes longer than that in **1a** but is slightly shorter than the Pt−N bond trans to the $sp^2$ carbon of the metalated phenyl ring, probably because an $sp^2$ carbon is a stronger donor. A similar trend is observed in **3a** and **3b**.

Complex **1a** displays nearly square planar coordination geometry. The *trans* C(1)−Pt(1)−N(3) bond angle is 174.85(9)°, a significant increase compared with that in the C^N^N-coordinated complexes (160°);[9] therefore, the angle strain caused by the fused five−five-membered ring is relieved in the C*N^N-coordinated platinum complex. The *N*-phenyl ring not being cyclometalated is nearly perpendicular to the coordination plane with a dihedral angle of 81.8°. A $\pi\cdots\pi$ interaction was found in the crystal packing, and the distance between the coordination planes of the adjacent two molecules was measured to be 3.450 Å. The stacking apparently takes a head to tail orientation of the two molecules so that they attract with each other through electron-deficient pyridine ring and electron-rich cyclometalated phenyl ring and minimize the steric effect of the perpendicular *N*-phenyl ring. There is no Pt···Pt interaction.

The complex **1b** crystallized as orange plates with the solvent molecule of dichloromethane in the crystal packing. There are two independent molecules in the unit cell. Molecule **A** (Figure 1) shows nearly square but distorted planar geometry with the cyclometalated N-phenyl ring slightly twisted out of the coordination plane. The other molecule (**B**) has more distorted coordination geometry than the **A**; specifically the cyclometalated N-phenyl ring in the molecule is more twisted out of the platinum-bipyridine coordination plane. In both molecules **A** and **B**, the ring of the phenylacetylide is only slightly twisted relative to the coordination plane. No significant $\pi\cdots\pi$ or Pt···Pt interaction could be detected.

In the unit cell of the complex **2b**, there are also two independent molecules. Both molecules display nearly planar coordination geometry; but the orientation of the phenyl ring of the phenylacetylide is quite different. In molecule **B** (Figure 1), the phenyl ring of the phenylacetylide ring is significantly more twisted forming a dihedral angle of 73.4° with the coordination plane, while the corresponding angle in the other molecule (molecule **A**) is only 24.2°. It is interesting to note that a relatively strong $\pi\cdots\pi$ interaction (3.422 Å) exists between two of the molecule **B**. Since both the N-phenyl group and the phenylacetylide ring are nearly perpendicular to the interacting coordination plane, they have to bend away from the plane (Figure 1, **2b** (molecule B)). This crystal packing


dx.doi.org/10.1021/ic400732g | Inorg. Chem. 2013, 52, 11711−11722

**Table 2. Photophysical Data for Complexes 1a, 1b, 2a, 2b, 3a, and 3b**

| | | 298 K[a] | | | 77 K[b] | | |
|---|---|---|---|---|---|---|---|
| complex | $\lambda_{abs}$[a] (nm) ($\varepsilon$, $M^{-1}$ $cm^{-1}$) | $\lambda_{em}$ (nm) | $\tau^0$ ($\mu$s) | $\phi^d$ (%) | $\lambda_{em}$ (nm) | $\tau$ ($\mu$s) | solid state $\lambda_{em}$[c] (nm) ($\tau$, $\mu$s) |
| **1a** | 274 (38674), 387 (6682), 469 (4659) | 615 | <0.5 | 0.1 | 568, 611 | 5.9 | 565 (6.8), 604 (9.6) |
| **1b** | 280 (43400), 402 (6067), 468 (4216) | 615 | <0.5 | 0.4 | 562, 610 | 7.5 | 600 (8.9) |
| **2a** | 271 (33262), 333 (9984), 417 (4877) | 523 | <0.5 | <0.1 | 499, 534, 573 | 19.8 | 502 (7.8), 532 (8.7), 571 (8.7) |
| **2b** | 276 (66222), 336 (13702), 415 (7811) | 521 | 8.6 | 43 | 497, 534, 575 | 10.5 | 502 (9.6), 531 (8.3), 570 |
| **3a** | 270 (17217), 305 (18150), 387 (3016), 496 (60) | 504, 540 | <0.5 | 3.5 | 495, 532, 570 | 9.8 | 534 (9.4), 572 (10.2) |
| **3b** | 277 (20070), 310 (13639), 355 (5093), 411 (4264), 497 (94) | 511, 534 | 5.2 | 62 | 495, 532, 568 | 5.3 | 548 (10.3) |

[a]Measurements were carried out in a solution of dichloromethane. [b]Measurements were carried out in a solution of 2-methyltetrahydrofuran. [c]Solid state spectra were measured with a pure powder sample at 298 K. [d]Quantum yields were measured in deoxygenated dichloromethane with quinine sulfate in 0.1 N $H_2SO_4$ ($\phi$ = 0.55) as the reference.

feature suggests considerable flexibility of these C*N^N-coordinated platinum complexes.

The tridentate C^N^N-coordinated platinum complexes **3a** and **3b** display nearly perfect planarity; but they deviates significantly from the square arrangement of the coordinating groups as indicated by small biting angles of C(1)−Pt(1)−N(3) (160.86°) and C(1A)−Pt(1)−N(3A) (159.8°) in **3a** and **3b**, respectively. There are two independent molecules in the unit cell of **3b** and both have very similar geometry. In the molecule **A**, the platinum and the cyclometalating ligand forms the coordination plane and the largest deviation of atoms from the calculated mean plane is 0.08 Å. The acetylide is not coplanar with the platinum and the C^N^N ligand with deviations of 0.168 and 0.374 Å for the two sp carbons, respectively, while the corresponding deviations in molecule **B** are 0.293 and 0.556 Å. Interestingly, in both of the molecules **A** and **B**, the phenyl ring of the phenylacetylide is nearly perpendicular to the coordination plane. The dihedral angle is 86.73° in molecule **A** and 85.28° in molecule **B**. A $\pi\cdots\pi$ interaction was found in the crystal packing of **3a** and the distance between the coordination planes of two adjacent molecules was measured to be 3.414 Å. The stacking takes a head to tail orientation and the two molecules attracts with each other through interaction of the electron-deficient moiety and the electron-rich moiety. There is no Pt···Pt interaction.

In **1a**, **1b**, and **2b**, the amino nitrogen forms strongest bond with the carbon of the N-pyridine ring, N(1)−C(7), and weakest bond with the carbon of the N-phenyl ring. This strong bonding may be attributed to the strong donor−acceptor conjugation between the lone pair of the nitrogen and the electron-deficient heteroaromatic ring assembly. The conjugation between the nitrogen and the phenyl is disrupted by the orthogonal relationship between the lone pair and the $\pi$ orbitals of the phenyl ring. A small but steady increase in N(1)−C(7) bond length from **1a** → **1b** → **2b** (1.377 → 1.381 →1.393 Å) might be related to the weakening of the electron acceptor by introducing the donating phenylacetylide group and poorer electron accepting pyrazolyl group.

**Photophysical Properties.** The photophysical data obtained for all complexes are listed in Table 2. The absorption and fluorescence emission spectra of ligands **L1**−**L3** are provided in the Supporting Information (Figures S1 and S2).

*Absorption.* The absorption spectra of the complexes **1a**, **1b**, **2a**, and **2b** are shown in Figure 2. All spectra show strong absorptions in the high-energy region and weaker absorptions in the low-energy region. The high-energy intense absorptions can be assigned as ligand based $^1\pi-\pi^*$ transitions, while the low energy absorptions that are not present in the absorption

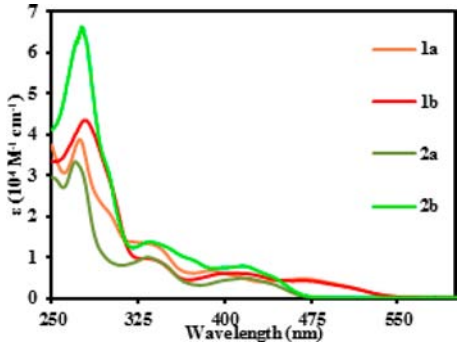


**Figure 2.** Absorption spectra of **1a**, **1b**, **2a**, and **2b** in dichloromethane.

spectra of the corresponding ligands can be assigned as charge transfer bands. The lowest energy absorptions of **2a** and **2b** display a significant blue-shift compared to those of **1a** and **1b**. This can be attributed to the replacement of the pyridyl ring by the pyrazolyl ring that is a poor electron acceptor.[5,14] The introduction of phenylacetylide does not cause drastic change in the absorption spectra except for the enhancement in the high energy region assigned to $^1\pi-\pi^*$ transitions.

The absorption of **3a** and **3b** showed some interesting features (Figure 3). The two complexes showed different low

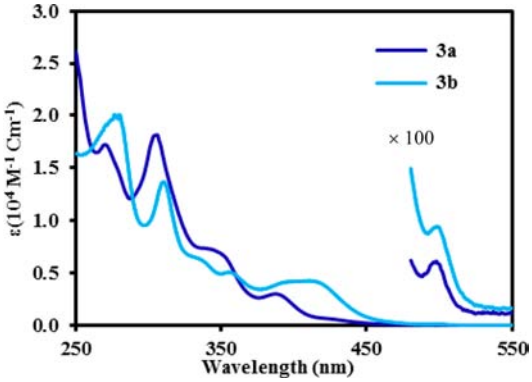


**Figure 3.** Absorption spectra of **3a** and **3b**. Inserted are expanded spectra (×100) showing the lowest energy triplet absorptions.

energy absorption bands. The less intense absorption at around 410 nm for the complex **3b** is apparently due to the introduction of phenylacetylide, while the lowest energy singlet absorption for **3a** is 387 nm. When expanding the absorption spectra in the low energy region, very weak absorptions at 496 (60 $M^{-1}$ $cm^{-1}$) and 497 nm (94 $M^{-1}$ $cm^{-1}$) were found for **3a**


dx.doi.org/10.1021/ic400732g | Inorg. Chem. 2013, 52, 11711−11722

and **3b**, respectively. These weak absorptions might be assigned as triplet ligand-centered transitions. Such triplet absorptions were not observed in the spectra of **1a**, **1b**, **2a**, and **2b**. Triplet ligand-centered absorptions are not frequently reported; but have been observed for tridentate N^C^N-coordinated[10a] and tetradentate C^N*N^C-coordinated[6] platinum complexes.

Solvent effects on the absorption spectra of the six complexes have been examined and the shifts of low energy absorption bands with the solvents are listed in Table S2 (Supporting Information). The low energy absorptions showed remarkable solvent dependence and shifted to the higher energy by up to 47 nm (2066 $cm^{-1}$) for **1a** as the polarity of the solvents increases from toluene to acetonitrile, indicating that these low energy transitions possess significant charge transfer character.

*Ambient Emission in Fluid.* At room temperature, both complex **1a** and **1b** displayed a weak and structureless emission in the red region (Figure 4). Although the complex **2a** with a chloride ligand was only weakly emissive (spectrum not shown in Figure 4), its phenylacetylide derivative **2b** was strongly emissive and emitted bright green light with a quantum yield of 43%. The acetylide ligand is a much stronger donor than the chloride, therefore inducing a stronger ligand field that raises the nonradiative MC state to higher energy.[16] Much weaker emission displayed by **1a** and **1b** may be explained by considering the energy gap law that rules the lower efficiency for the lower energy emission. As a comparison to the C*N^N-coordinated platinum complex **2a**, the C^N^N-coordinated complexes **3a** was found to emit green light with an appreciable quantum yield of 3.5%. When the chloride in **3a** was replaced with phenylacetylide, the quantum yield of **3b** jumped to 62%. It should be mentioned that the phosphorescence efficiency of C^N^N type of cyclometalated platinum complexes has been reported to be generally low[10,17] (<10%). Only in the cases where extended $\pi$-conjugation was introduced to the cyclometalating ligand were higher quantum yields reported to be attributed to the rigid structure of extended $\pi$-conjugation.[18] It has also been suggested that the geometric distortion of the triplet state of the C^N^N-coordinated platinum complex based on 6-phenyl-2,2′-bipyridyl ligand is the main cause of its low quantum efficiency.[19] Higher quantum efficiency displayed by **3b** may be attributed to the more rigid fused five−five-membered metallacycle and minimal geometric distortion of the triplet state.

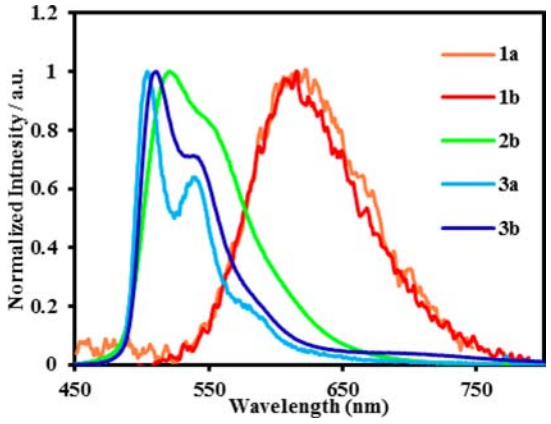


**Figure 4.** Emission spectra of **1a**, **1b**, **2b**, **3a**, and **3b** in dichloromethane at 298 K.

Concentration quenching (self-quenching) was observed for both **2b** and **3b** in the range of $10^{-6}$ to $10^{-4}$ M. The intensity of the emission for both **2b** and **3b** decreases gradually as the concentration of the complexes increases. The concentration quenching may be resulted from the excimer formation rather than aggregation of the molecule at its ground state since the absorptions of the complexes obeyed the Beer's law in the range of $10^{-6}$ to $10^{-4}$ M. The observed decay rate was fit to a Stern−Volmer equation (eq 1),[20] where $k_q$ is the self-quenching (excimer formation) rate constant, [Pt] is the concentration of the platinum complex, and $k_0$ is the decay rate for the monomer complex.

$$k_{obs} = k_q[Pt] + k_0 \quad (1)$$

The self-quenching rate constants $k_q$ were $7.4 \times 10^7$ and $2.3 \times 10^9$ $M^{-1}s^{-1}$ for **2b** and **3b**, respectively. The quenching constant of **3b** is well within the range reported for other similar emissive platinum complexes.[20,6] The quenching constant for **2b** is much smaller than that of **3b**, which may be attributed to the fact that **2b** is not as planar as **3b**, making it more difficult to form the excimer or the aggregates through a $\pi$ interaction. As revealed in the crystal packing of **2b**, the $\pi-\pi$ interaction accompanies further geometric distortion of the molecules. The monomer emission lifetime ($\tau^0$) was extrapolated to be 8.6 and 5.2 $\mu$s ($1/k_0$) for **2b** and **3b**, respectively. The long lifetime suggest a ligand-centered transition state with a metal-to-ligand charge transfer (MLCT) admix that promotes the phosphorescent emission.

The radiative and nonradiative rate constants were estimated from the luminescent quantum yield ($\phi$) and lifetime ($\tau$) of the phosphorescent complex according to eqs 2 and 3, respectively

$$k_r = \phi\tau^{-1} \quad (2)$$

$$k_{nr} = k_r(\phi^{-1} - 1) \quad (3)$$

where $k_r$ and $k_{nr}$ are the radiative and nonradiative rate constant, respectively. The radiative constants for **2b** and **3b** were $4.99 \times 10^4$ and $1.3 \times 10^5$ $s^{-1}$, respectively. The nonradiative decay constants for **2b** and **3b** were $6.6 \times 10^4$ and $6.1 \times 10^4$ $s^{-1}$, respectively. Since both **2b** and **3b** have similar nonradiative decay rate constants, the higher quantum efficiency of **3b** is due to its fast radiative decay of the excited state.

The solvents had very small and uncharacteristic effects on the emissions of **1a**, **1b**, **2a**, and **2b** (Table S2, Supporting Information). In contrast, the solvent effect on the emissions of **3a** and **3b** showed some noteworthy tends. In both cases, a negative solvatochromic effect on the emission was observed, namely a shift of emission maximum to high energy as the polarity of the solvents increases; however the magnitude of the solvatochromic shifts is drastically different and a much greater solvatochromic shift was observed for **3b**. When the solvents were changed from toluene to acetonitrile, the emission maximum was shifted from 511 to 505 nm for **3a** (232 $cm^{-1}$ shift) and from 521 to 499 nm for **3b** (846 $cm^{-1}$ shift). Emission of **3a** displays a highly structured spectrum with a vibronic progression of 1322 $cm^{-1}$, indicating an LC transition state involving the aromatic cyclometalated ligand. The larger solvatochromic shift and smoother band shape of **3b** suggested a transition state of more charge-transfer character that leads to more significant dipole moment change during the excitation.


dx.doi.org/10.1021/ic400732g | *Inorg. Chem.* 2013, 52, 11711−11722

The nature of the charge transfer can be either MLCT or LLCT (acetylide to the pyrazolylpyridine receptor) or both.

*Emission in Rigid Glass at 77 K.* All complexes are emissive in rigid glass at 77 K and estimated lifetimes of the emissions are in the micro second regime, indicating that they are phosphorescent emissions. All complexes displayed highly structured spectra with vibronic progressions of about 1300−1400 $cm^{-1}$. The emission can be assigned as primarily LC states based on the structured spectra and relatively long lifetimes (5.3−19.8 $\mu s$). It is noteworthy that the emission spectra are almost identical for **1a** and **1b**, **2a** and **2b**, or **3a** and **3b**, respectively, indicating that the excited states are primarily localized on the tridentate cyclometalated ligands (Figure 5).

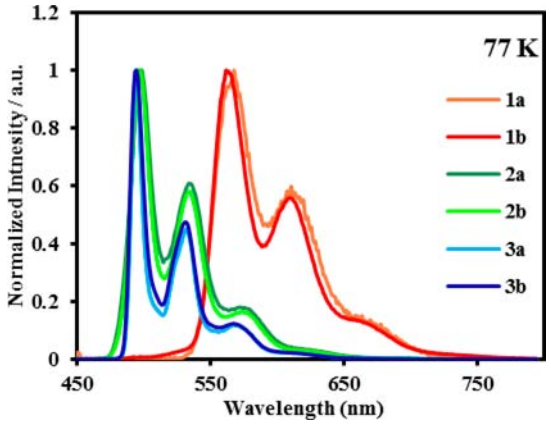


**Figure 5.** Emission spectra of **1a**−**3a** and **1b**−**3b** in rigid glass at 77 K.

The monoanionic ligand chloride or phenylacetylide had little effect on the LC states. The Huang−Rhys ratios ($S = I_{1-0}/I_{0-0}$, estimated from the relative peak intensities of vibrational emission bands) of the emissions is smaller for **3a** (0.45) and **3b** (0.47) than those of **1a** (0.6), **1b** (0.56), **2a** (0.61), and **2b** (0.58). A higher Huang−Rhys ratio suggests larger distortion of the excited states. Larger rigidochromic shifts were observed for **1a** (1345 $cm^{-1}$), **1b** (1533 $cm^{-1}$), **2a** (920 $cm^{-1}$) and **2b** (927 $cm^{-1}$) than those of **3a** (361 $cm^{-1}$) and **3b** (632 $cm^{-1}$). Based on the fact that the emissions of **1a** and **1b** in solution have nearly identical energy and shape, they can be assigned as a primarily LC state localized on the tridentate ligand.

*Emission in solid state.* All complexes are emissive in solid state at ambient temperature and lifetimes of the emissions are also in the micro second regime. The emissions of **1a**, **1b**, **2a**, and **2b** are structured and very similar to their emission in rigid glass except for more intensified vibrational bands (Figure 6). The emissions of **3a** and **3b** displayed broad spectra and showed red shift in the solid state, probably because of the intermolecular interaction in the solid state.

**Theoretical Calculations.** In order to further understand the nature of excited states and the emissions in different environments, density functional theory (DFT) and time-dependent DFT (TDDFT) calculations were performed on the complexes **1a**−**3a** and **1b**−**3b**. Since the X-ray crystallography revealed two conformational isomers in the crystals of **1b**−**3b**, the DFT calculations were performed on both conformer **A**, in which the phenyl ring of the acetylide is coplanar with the coordination plane, and conformer **B** with the phenyl group being perpendicular. The conformer **A** was predicted to be more stable than **B**, but the calculated energy difference between the two conformers are very small (<1 kcal/mol).

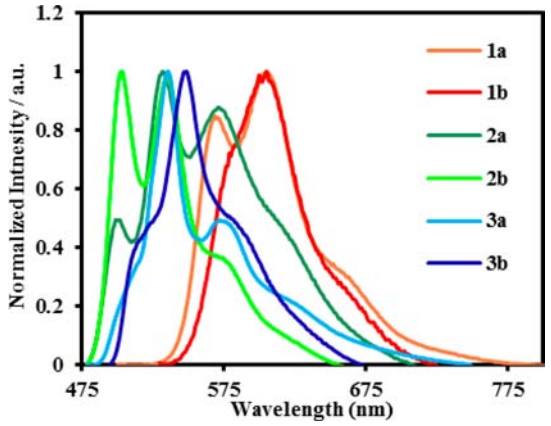


**Figure 6.** Emission spectra of **1a**−**3a** and **1b**−**3b** in solid state (pure powder).

Owing to the cylindrical geometry of the carbon−carbon triple bond, a free rotation of the phenyl ring at ambient temperature may be expected.

*DFT Calculations.* The selected molecular orbital energies and the contribution of platinum to the MOs are provided in Supporting Information (Table S3). The orbital densities of selected MOs are provided in the Supporting Information (Figures S5 and S6). The orbital densities for the HOMO and LUMO are depicted in Figure 7. The HOMOs of **1a**, **2a**, and **3a** are mainly localized on the platinum and metalated phenyl ring. The HOMOs of **1b-A**, **1b-B**, and **2b-A** are spread over the metalated phenyl ring, the platinum, and the phenylacetylide, whereas for **2b-B** there is little contribution from the phenylacetylide. The HOMOs of **3b-A** and **3b-B** are localized on the phenylacetylide and the platinum. All structures have their LUMOs localized on the electron-deficient heteroaromatic rings as expected.

The geometry of the lowest triplet state ($T_1$) was also optimized for **1a-3a** and **1b-3b**, which does not show any significant change compared to the corresponding $S_0$ geometry. The root-mean-squares of change in geometry between optimized singlet and triplet states for **1a**, **1b-A**, **1b-B**, **2a**, **2b-A**, **2b-B**, **3a**, **3b-A**, and **3b-B** are 0.0099, 0.0267, 0.0004, 0.0015, 0.5956, 0.0425, 0.0011, 0.0033, and 0.0005 Å, respectively, which is generally in line with the Huang−Rhys ratios as discussed before. The selected molecular orbital energies and the contribution of platinum to the MOs are provided in the Supporting Information (Table S4). The orbital densities for selected MOs are depicted in Figures S7 and S8 (Supporting Information). The spin densities of the triplet states for **1a**, **2a**, **3a**, **1b-A**, **2b-A**, and **3b-A** were calculated and their contour plots are shown in Figure 8. All structures but **3b-A** have the spin density distributed mostly in the tridentate ligand with a smaller portion on the platinum, indicative of a ligand-centered state. In **3b-A**, considerable spin density in the phenyl acetylide indicates a significant ligand-to-ligand charge transfer (LLCT, phenylacetylide to tridentate ligand) character.

*Time-Dependent DFT Calculations.* TDDFT calculations were performed to gain insightful understanding of the nature of the transitions of complexes. Selected singlet−singlet transitions are listed in Table S5 (Supporting Information). The lowest singlet transitions of **1a,b**, **2a,b**, and **3a,b** are listed in Table 3. The experimental lowest-energy absorptions are included for comparison. Except for those of **3b-A** and **3b-B**, the lowest singlet excited state for all other structures is mainly


dx.doi.org/10.1021/ic400732g | *Inorg. Chem.* 2013, 52, 11711−11722

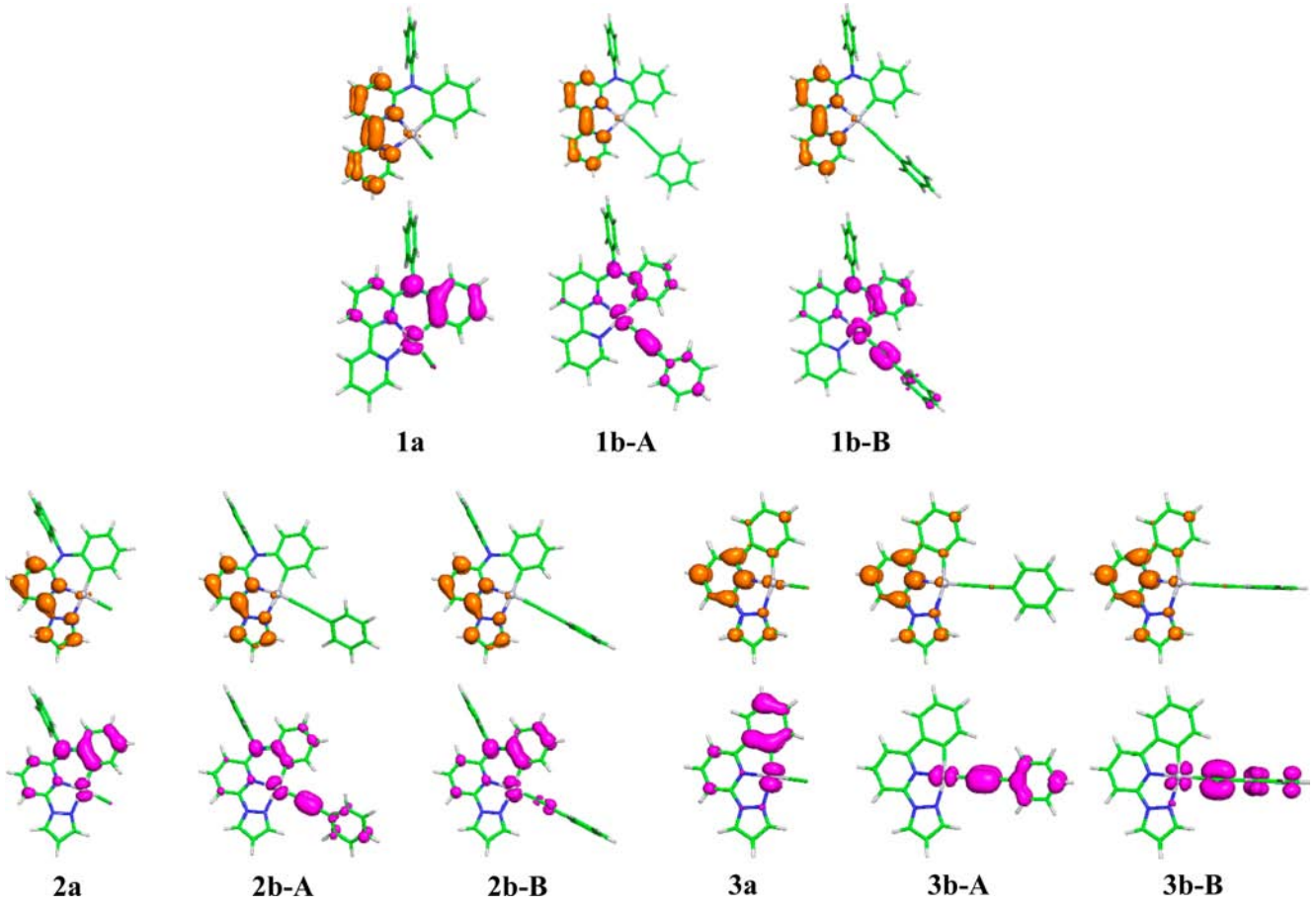


**Figure 7.** Calculated orbital density for the HOMO (magenta) and LUMO (orange) of **1a**−**3a** and **1b**−**3b** at their optimized $S_0$ geometries.

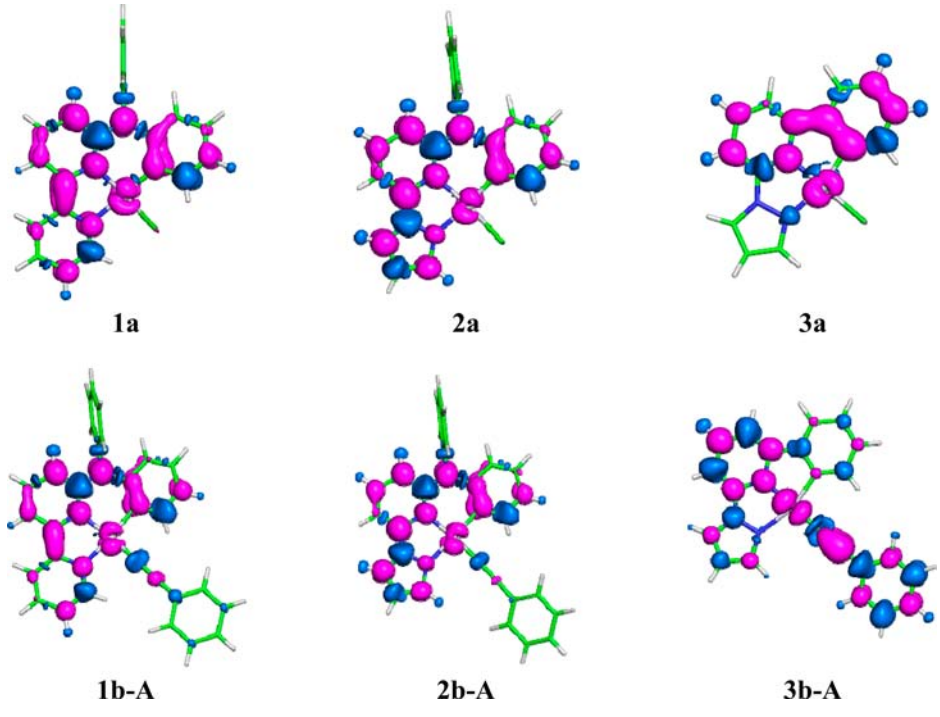


**Figure 8.** Spin densities of the lowest triplet states ($T_1$) of **1a**−**3a**, **1b-A**, **2b-A**, and **3b**-A.

derived from HOMO→LUMO transitions. It is interesting to note that **3b** has the lowest singlet state derived from mainly HOMO-1→LUMO transition. According to the orbital density of those MOs (Figure 7 and Figure S6 in Supporting Information), the transitions can be assigned as a mixed state involving one or more of the following charge transfer


dx.doi.org/10.1021/ic400732g | *Inorg. Chem.* 2013, 52, 11711−11722

**Table 3. TD-DFT g09 m62x/def2-pvtz Lowest Singlet Excitation States of 1a−3a and 1b−3b at Their Optimized Geometries of the Ground States**

| compd | state | main component | energy, eV (nm) | oscillator | experiment $\lambda_{abs}$ (nm) |
|---|---|---|---|---|---|
| **1a** | $S_1$ | HOMO→ LUMO | 3.20 (388) | 0.1321 | 469 |
| **1b-A** | $S_1$ | HOMO→ LUMO | 3.11 (398) | 0.1648 | 468 |
| **1b-B** | $S_1$ | HOMO→ LUMO | 3.19 (389) | 0.1438 | 468 |
| **2a** | $S_1$ | HOMO→ LUMO | 3.54 (350) | 0.1855 | 417 |
| **2b-A** | $S_1$ | HOMO→ LUMO | 3.52 (352) | 0.2320 | 415 |
| **2b-B** | $S_1$ | HOMO→ LUMO | 3.56 (348) | 0.2139 | 415 |
| **3a** | $S_1$ | HOMO→ LUMO | 3.41 (363) | 0.0149 | 387 |
| **3b-A** | $S_1$ | HOMO-1→ LUMO | 3.38 (366) | 0.0157 | 411 |
| **3b-B** | $S_1$ | HOMO-1→ LUMO | 3.42 (362) | 0.0086 | 411 |

transitions MLCT (platinum to tridentate ligand), ILCT (tridentate ligand) and LLCT (phenylacetylide to tridentate ligand). The order of computed energies (**1a,b** < **3a,b** < **2a,b**) of $S_0 \rightarrow S_1$ transitions does not agree exactly with observed lowest energy absorptions (**1a,b** < **2a,b** < **3a,b**) for **1a−3a** and **1b−3b**. The discrepancy between **2a,b** and **3a,b** might be attributed to their different structural types that have different sensitivity to the computational methods used. The calculated lowest singlet energies for **1a,b** and **2a,b** are significantly overestimated. It should also be pointed out that the 387 nm may not be the true lowest energy absorption for **3a** since there is a shoulder at around 410 nm in the spectrum (Figure 3).

The calculated energies and main components for the lowest triplet excited states are listed in Table 4. Experimental lowest triplet absorptions and the phosphorescent emission maxima are also provided as a comparison. All the triplet excited states have multiple one-electron excitation configurations but only the main components with the coefficient's absolute value being equal to or greater than 0.3 are listed in the table. According to the orbital densities of the MOs (Figures S7 and S8, Supporting Information), the first triplet state ($T_1$) for **1a−3a** can be characterized as a LC state localized on the tridentate ligand with an MLCT admixture. The first triplet state of **1b-A** and **2b-A** can be assigned as a mixed state involving ILCT, LLCT, and MLCT, but that of **3b-A** has much greater LLCT character, which is very similar to recently reported alkynylplatinum complexes based on tridentate N-hetereocyclic carbene ligand.[21] The $T_1$ state for **1b-B**, **2b-B**, and **3b-B** can be assigned as a mixed state involving ILCT and MLCT, similar to **1a−3a**. Although the calculated $T_1$ energies of **3a** and **3b** are very close to the experimental triplet absorptions and phosphorescent emissions, those for **1a-b** and **2a-b** are significantly overestimated compared to the observed emissions. The assignment of room temperature emissions of **1b−3b** in solution can be complicated by the fact that the different conformers resulted from the rotation of the phenyl ring of the phenylacetylide ligand behavior differently. However, the emissions **1b−3b** in the frozen glass can be confidently assigned as a LC state localized on the tridentate ligand as they are nearly identical, both in energy and in shape, to the emissions of **1a−3a**, respectively, which implies that the molecules **1b−3b** in the rigid matrix might adopt the perpendicular conformation **B** in which the participation of the phenyl group of the acetylide is prohibited due to its orthogonal relationship with the coordination plane.

**Table 4. TD-DFT g09 m62x/def2-pvtz Lowest Triplet Excitation States of 1a−3a and 1b−3b at Their Optimized Geometry of the Lowest Triplet State $T_1$**

| compd | state | main component | coeff | energy, eV (nm) | exptl $\lambda_{abs}$ (nm) | exptl $\lambda_{em}$ (nm) |
|---|---|---|---|---|---|---|
| **1a** | $T_1$ | HOMO → LUMO | 0.64 | 2.25 (552) | | 615 |
| **1b-A** | $T_1$ | HOMO-1 → LUMO | 0.30 | 2.29 (542) | | 615 |
| | | HOMO → LUMO | 0.57 | | | |
| **1b-B** | $T_1$ | HOMO → LUMO | 0.57 | 2.29 (542) | | 615 |
| **2a** | $T_1$ | HOMO → LUMO | 0.63 | 2.57 (483) | | 523 |
| **2b-A** | $T_1$ | HOMO-1 → LUMO | −0.35 | 2.64 (470) | | 521 |
| | | HOMO → LUMO | 0.53 | | | |
| **2b-B** | $T_1$ | HOMO → LUMO | 0.61 | 2.60 (478) | | 521 |
| **3a** | $T_1$ | HOMO→ LUMO | 0.63 | 2.42 (512) | 496 | 504 |
| **3b-A** | $T_1$ | HOMO → LUMO | 0.57 | 2.56 (484) | 497 | 511 |
| **3b-B** | $T_1$ | HOMO-1 → LUMO | 0.60 | 2.69 (462) | 497 | 511 |

## SUMMARY

The C*N^N and C^N^N-coordinated platinum complexes have been synthesized and their structural and photophysical properties have been investigated. TDDFT calculations have been carried out to elucidate the nature of excited states and the origin of phosphorescence emissions. Both **2b** and **3b** emited intensely bright green light at room temperature. With this report, we have completed design, synthesis, structure, and photophysical characterization of a series of cyclometalated platinum complexes featuring in a fused five-six-membered metallacycle, which are designed by introducing an amine linker to more conventional C^N^N and N^C^N types of cyclometalating ligands. The design allows many options in engineering a ligand to achieve desired properties of the cyclometalated complexes. The synthetic strategies introduced in these studies, particularly the use of the combination of Pd-catalyzed C−C and Pd or Cu-catalyzed C−N bond cross-coupling reactions are generally applicable to the synthesis of other similar ligands.

Through these studies on the cyclometalated platinum complexes based on tridentate CNN and NCN ligands, the geometrical and electronic effects on the photophysical properties, particularly the phosphorescence efficiency, can be summarized as follows. The introduction of five-six-membered metallacycle improves the square geometry of the platinum complexes but may increase the flexibility of the molecules, which has contradictory effects on the quantum efficiency. Such geometrical modification alone seems insufficient to induce such a large d orbital splitting that the nonradiative *d*−*d* transition becomes thermally inaccessible, because the (C^N*N)PtCl and (C*N^N)PtCl were found to be less


dx.doi.org/10.1021/ic400732g | Inorg. Chem. 2013, 52, 11711−11722

emissive than their corresponding (C^N^N)PtCl. More importantly, the introduction of an acetylide ligand is still necessary to achieve high efficiency. In this context, the superior quantum efficiencies displayed by (N^C^N)PtCl and (N*C^N)PtCl over those of (C^N^N)PtCl, (C^N*N)PtCl, and (C*N^N)PtCl are quite remarkable. On the other hand, both N^C^N and N*C^N-coordinated platinum complexes display comparable and generally high quantum efficiency, which indicates that the positive electronic effect of rectified square coordination may offset the negative geometrical effect of increased flexibility. Finally, the N^C^N[9]- and N*C^N-coordinated[5] platinum complexes have demonstrated decent to high phosphorescence efficiency in low energy emission beyond green. In contrast, complexes based on C^N^N[10,17,18] ligand that emits efficiently in the orange to red region have not been reported.

## EXPERIMENTAL SECTION

**Synthesis.** All reactions involving moisture- and/or oxygen-sensitive organometallic complexes were carried out under nitrogen atmosphere and anhydrous conditions. Tetrahydrofuran (THF) and 2-methyltetrahydrofuran were distilled from sodium and benzophenone under nitrogen before use. All other anhydrous solvents were purchased from Aldrich Chemical Co. and were used as received. All other reagents were purchased from chemical companies and were used as received. Mass spectra were measured on a Waters spectrometer. NMR spectra were measured on a Bruker 400 or a Varian 500 spectrometer. Spectra were taken in $CDCl_3$ or $CD_2Cl_2$ using tetramethylsilane as standard for $^1H$ NMR chemical shifts and the solvent peak ($CDCl_3$, 77.0 ppm; $CD_2Cl_2$, 53.8 ppm) as standard for $^{13}C$ NMR chemical shifts. Elemental analyses were performed at Atlantic Microlab, Inc., Norcross, GA.

**Preparation of L1.** To a 25 mL flask were charged 6-bromo-2,2′-bipyridine (470 mg, 2 mmol), diphenylamine (508 mg, 3 mmol), $Pd(dba)_2$ (46 mg, 0.08 mmol), DPPF (44 mg, 0.08 mmol), sodium *tert*-butoxide (231 mg, 2.4 mmol), and toluene (5 mL), and the mixture was refluxed for 24 h. After being cooled to room temperature, the reaction mixture was poured into water, and the aqueous phase was extracted with ethyl acetate (EtOAc) (3 × 35 mL). The combined organic extracts were washed with water (50 mL) and then brine (50 mL) and dried over $MgSO_4$. The mixture was filtered, concentrated in vacuo, and purified by chromatography on silica gel with a mixture of hexanes and ethyl acetate (7:1 v/v) to provide an off-white solid, 575 mg, yield 89%: $^1H$ NMR (400 MHz, $CDCl_3$) $\delta$ 8.61(d, $J$ = 4.75 Hz, 1H), 7.99 (dt, $J$ = 8 Hz, 1 Hz, 1H), 7.92 (dd, $J$ = 7.5 Hz, 0.7 Hz, 1H), 7.65 (td, $J$ = 8.0 Hz, 1.8 Hz, 1H), 7.57 (t, $J$ = 8.3 Hz, 1H), 7.37−7.33 (m, 4H), 7.28−7.25 (m, 4H), 7.22−7.19 (m, 1H), 7.18−7.13 (m, 2H), 6.73(dd, $J$ = 8 Hz, 0.7 Hz, 1H); $^{13}C$ NMR (100 MHz, $CDCl_3$) $\delta$ 158.04, 156.29, 154.05, 148.86 (2C), 145.95, 138.30, 136.79, 129.20 (4C), 126.52 (4C), 124.49 (2C), 123.40, 121.09, 113.30, 113.04. Anal. Calcd. for $C_{22}H_{17}N_3$: C, 81.71; H, 5.30; N, 12.99. Found: C, 81.76; H, 5.39; N, 12.89.

**Preparation of L2. General Procedure A.** To a 25 mL flask were charged 6-bromo-*N*,*N*-diphenylpyridin-2-amine (218 mg, 0.7 mmol), pyrazole (68 mg, 1 mmol), $K_2CO_3$ (207 mg, 1.5 mmol), CuI (13 mg, 0.07 mmol), trans-*n*,*n*′-dimethylcyclohexane-1,2-diamine (25 mg, 0.175 mmol), and toluene (5 mL). The mixture was refluxed for 24 h. After being cooled to room temperature, the reaction mixture was poured into water, and the aqueous phase was extracted with ethyl acetate (EtOAc) (3 × 30 mL). The combined organic extracts were washed with water (50 mL) and brine (50 mL) and dried over $MgSO_4$. The mixture was filtered, concentrated in vacuo, and purified by chromatography on silica gel with a mixture of hexanes and ethyl acetate (7:1 v/v) to provide an off-white solid, 214 mg, yield 98%: $^1H$ NMR (500 MHz, $CDCl_3$) $\delta$ 8.07 (d, $J$ = 2.5 Hz, 1H), 7.65 (d, $J$ = 1.5 Hz, 1H), 7.53 (t, $J$ = 8.5 Hz, 1H), 7.40−7.33 (m, 5H), 7.27−7.25 (m, 4H), 7.18 (t, $J$ = 7.5 Hz, 2H), 6.53 (d, $J$ = 8.5 Hz, 1H), 6.30 (t, $J$ = 2.5 Hz, 1H); $^{13}C$ NMR (100 MHz, $CDCl_3$) $\delta$ 157.15, 149.66, 145.37, 141.70 (2C), 139.86, 129.27 (4C), 127.09, 126.83 (4C), 125.00 (2C), 109.31, 107.18, 102.85. Anal. Calcd for $C_{20}H_{16}N_4$: C, 76.90; H, 5.16; N, 17.94. Found: C, 76.85; H, 5.14; N, 18.00.

**Preparation of L3.** This ligand was prepared from 2-bromo-6-phenylpyridine (702.3 mg, 3 mmol) following general procedure A. The product was purified by chromatography on silica gel with a mixture of dichloromethane and hexanes (2:1 v/v to 4:1 v/v) to provide a colorless solid, 298.7 mg, yield 45%: $^1H$ NMR (500 MHz, $CDCl_3$) $\delta$ 8.73 (d, $J$ = 2 Hz, 1H), 8.06 (dd, $J$ = 8.5 Hz, 1.5 Hz, 2H), 7.92 (d, $J$ = 7.5 Hz, 1H), 7.82 (t, $J$ = 8.5 Hz, 1H), 7.76 (d, $J$ = 1.5 Hz, 1H), 7.59 (dd, $J$ = 7.5 Hz, 1 Hz, 1H), 7.50−7.40 (m, 3H), 6.47 (dd, $J$ = 3 Hz, 1.5 Hz, 1H); $^{13}C$ NMR (100 MHz, $CDCl_3$) $\delta$ 155.19, 151.31, 142.00, 139.46, 138.39, 129.37, 128.77(2C), 127.10, 126.88 (2C), 117.68, 110.62, 107.61. Anal. Calcd for $C_{14}H_{11}N_3$: C, 76.00; H, 5.01; N, 18.99. Found: C, 76.04; H, 5.03; N, 19.09.

**Preparation of Platinum Complex 1a. General Procedure B.** To a 50 mL dry, argon-flushed flask were charged ligand **L1** (161.6 mg, 0.5 mmol), $K_2PtCl_4$ (207.6 mg, 0.5 mmol), and glacial acetic acid (20 mL). The mixture was degassed and refluxed under argon for 22 h. After the mixture was cooled to room temperature, the orange precipitates were collected by filtration, washed with water, and dried in air. The crude material was purified by flash chromatography on silica gel with dichloromethane. The compound was further recrystallized from dichloromethane and hexanes to give an orange solid, 204 mg, yield 74%: $^1H$ NMR (500 MHz, $CD_2Cl_2$) $\delta$ 9.94 (d, $J$ = 6 Hz, 1H), 8.71 (dd, $J$ = 7.5 Hz, 2 Hz, $^3J_{Pt-H}$ = 27 Hz, 1H), 8.16−8.10 (m, 2H), 7.75−7.68 (m, 4H), 7.63−7.59(m, 2H), 7.38 (d, $J$ = 7.55 Hz, 2H), 6.89−6.83 (m, 2H), 6.75 (d, $J$ = 9 Hz, 1H), 6.37 (dd, $J$ = 8 Hz, 2 Hz, 1H); $^{13}C$ NMR was not obtained due to poor solubility. Anal. Calcd. for $C_{22}H_{16}N_3ClPt$: C, 47.79; H, 2.92; N, 7.60. Found: C, 48.02; H, 2.81; N, 7.63.

**Complex 2a.** This complex was prepared from **L2** (78.1 mg, 0.25 mmol) following general procedure B. The crude material was purified by flash chromatography on silica gel with dichloromethane. The compound was further recrystallized from dichloromethane and hexanes to give a yellow solid, 132.5 mg, yield 98%: $^1H$ NMR (500 MHz, $CD_2Cl_2$) $\delta$ 8.58 (dd, $J$ = 7 Hz, 3 Hz, $^3J_{Pt-H}$ = 28 Hz, 1H), 8.32−8.31 (m, 2H), 7.71−7.58 (m, 4H), 7.36−7.34 (m, 2H), 7.04 (d, $J$ = 8 Hz, 1H), 6.86−6.83 (m, 3H), 6.38 (d, $J$ = 9 Hz, 1H), 6.28−6.26 (m, 1H). $^{13}C$ NMR (125 MHz, $CD_2Cl_2$) $\delta$144.21, 143.64, 140.89, 139.04, 136.02, 134.22, 131.82(2C), 130.69(2C), 129.49, 128.45, 124.38, 118.05, 115.47, 114.85, 110.37, 100.54 (only partial carbon signals were observed because of poor solubility). Anal. Calcd for $C_{20}H_{15}N_4ClPt$: C, 44.33; H, 2.79; N, 10.34. Found: C, 44.38; H, 2.62; N, 10.32.

**Complex 3a.** This complex was prepared from **L3** (110.6 mg, 0.5 mmol) following general procedure B. The crude material was purified by flash chromatography on silica gel with dichloromethane. The compound was further recrystallized from dichloromethane and hexanes to give a yellow solid, 132.1 mg, yield 57%: $^1H$ NMR (500 MHz, $CD_2Cl_2$) $\delta$ 8.21 (d, $J$ = 3 Hz, 1H), 7.94 (t, $J$ = 8.5 Hz, 2H), 7.65 (d, $J$ = 7.5 Hz, $^3J_{Pt-H}$ = 30.5 Hz, 1H), 7.44−7.42 (m, 2H), 7.26−7.21 (m, 2H), 7.13 (td, $J$ = 7.5 Hz, 1.5 Hz, 1H), 6.84 (t, $J$ = 3 Hz, 1H). $^{13}C$ NMR was not obtained due to poor solubility. Anal. Calcd for $C_{14}H_{10}N_3ClPt$: C, 37.30; H, 2.24; N, 9.32. Found: C, 37.41; H, 2.27; N, 9.28.

**Preparation of Platinum Complex 1b. General Procedure C.** To a 25 mL dry, argon-flushed flask were charged complex **1a** (127 mg, 0.23 mmol), phenylacetylene (76.9 $\mu$L, 0.7 mmol), CuI (3.5 mg, 0.018 mmol), $Et_3N$ (3 mL), and dichloromethane (20 mL). The mixture was stirred under argon at room temperature for 27 h. The crude material was purified by flash chromatography on silica gel with dichloromethane to give a yellow solid, 135.7 mg, yield 95%: $^1H$ NMR (500 MHz, $CD_2Cl_2$) $\delta$ 10.11 (d, $J$ = 5 Hz, 1H), 9.10 (dd, $J$ = 7.5 Hz, 2 Hz, $^3J_{Pt-H}$ = 39 Hz, 1H), 8.18 (d, $J$ = 8 Hz, 1H), 8.11 (t, $J$ = 8 Hz, 1H), 7.75−7.58 (m, 6H), 7.55 (d, $J$ = 7.5 Hz, 2H), 7.38 (d, $J$ = 8 Hz, 2H), 7.31 (t, $J$ = 7.5 Hz, 2H), 7.19 (t, $J$ = 8 Hz, 1H), 6.88 (t, $J$ = 7 Hz, 1H), 6.83 (t, $J$ = 7.5 Hz, 1H), 6.78 (d, $J$ = 9 Hz, 1H), 6.44 (d, $J$ = 8.5 Hz, 1H). $^{13}C$ NMR (125 MHz, $CD_2Cl_2$) $\delta$ 156.81, 154.60, 150.99, 149.20, 145.26, 144.51, 140.43, 137.80, 135.12, 131.73 (2C), 131.67 (2C),


dx.doi.org/10.1021/ic400732g | Inorg. Chem. 2013, 52, 11711−11722

131.01 (2C), 129.20 (2C), 128.36 (2C), 126.49, 125.43, 124.03, 122.41, 121.92, 120.75, 119.13, 118.66, 114.56, 100.43. Anal. Calcd for $C_{30}H_{21}N_3Pt{\cdot}0.5CH_2Cl_2$: C, 55.42; H, 3.35; N, 6.36. Found: C, 55.67; H, 3.25; N, 6.39.

**Complex 2b.** This complex was prepared from **1b** (124.6 mg, 0.23 mmol) following general procedure C. The crude material was purified by flash chromatography on silica gel with dichloromethane to give a yellow solid, 68 mg, yield 49%: $^1$H NMR (500 MHz, $CD_2Cl_2$) $\delta$ 8.93 (dd, $J$ = 7 Hz, 2 Hz, $^3J_{Pt-H}$ = 49.5 Hz, 1H), 8.39 (d, $J$ = 2 Hz, 1H), 8.33 (d, $J$ = 3 Hz, 1H), 7.71−7.64 (m, 3H), 7.60 (t, $J$ = 7.5 Hz, 1H), 7.51 (d, $J$ = 7.5 Hz, 2H), 7.36 (d, $J$ = 7.5 Hz, 2H), 7.29 (t, $J$ = 8 Hz, 2H), 7.18 (t, $J$ = 7.5 Hz, 1H), 7.06 (d, $J$ = 5 Hz, 1H), 6.87−6.80 (m, 2H), 6.78 (t, $J$ = 2.5 Hz, 1H), 6.42 (d, $J$ = 9 Hz, 1H), 6.36 (dd, $J$ = 8 Hz, 1.5 Hz, 1H); $^{13}$C NMR (125 MHz, $CD_2Cl_2$) $\delta$ 177.95, 170.58, 148.71, 144.71, 144.21, 142.08, 136.61, 134.43, 134.37, 134.35, 131.85 (2C), 131.75 (2C), 130.82 (2C), 129.31, 128.50, 128.32 (2C), 125.41, 124.11, 122.21, 118.85, 116.53, 114.57, 110.48, 100.24. Anal. Calcd for $C_{28}H_{20}N_4ClPt$: C, 55.35; H, 3.32; N, 9.22. Found: C, 55.09; H, 3.31; N, 9.15.

**Complex 3b.** This complex was prepared from **1c** (45.2 mg, 0.1 mmol) following general procedure C. The crude material was purified by flash chromatography on silica gel with a mixture of dichloromethane and ethyl acetate (50:1 v/v) to give orange solid, 29 mg, yield 56%: $^1$H NMR (500 MHz, $CD_2Cl_2$) $\delta$ 8.21(d, $J$ = 3 Hz, 1H), 8.03 (d, $J$ = 2 Hz, 1H), 7.96−7.92 (m, 2H), 7.51−7.45 (m, 4H), 7.30−7.26 (m, 3H), 7.25−7.05 (m, 3H), 6.75 (t, $J$ = 2.5 Hz, 1H); $^{13}$C NMR (125 MHz, $CD_2Cl_2$) $\delta$ 148.37, 146.51, 144.67, 144.21, 140.85, 140.45, 138.83, 138.18, 134.23, 131.98 (2C), 131.67, 130.37, 128.33 (2C), 125.44, 125.24, 124.00, 115.84, 110.51, 106.32, 105.18. Anal. Calcd for $C_{22}H_{15}N_3Pt$: C, 51.16; H, 2.93; N, 8.14. Found: C, 51.45; H, 2.85; N, 8.25.

**DFT Calculations.** All geometry optimizations were performed with DMol3[22] using the Tsuneda−Suzumura−Hirao[23] exchange-correlation energy-density functional. The base set was a double numerical plus double polarization numerical basis set generated by us. Relativistic effects were included using the all-electron-scattering theoretic approach to scalar relativistic corrections on bonding.[24] All other calculations were performed with Gaussian 09 using the m062x exchange-correlation energy-density functional. The basis set for Pt was the def2-tzvp[25] basis set while the 6-311g* basis set was used for all other atoms. The solvation model COSMO[26] was used to simulate the solvent effect of dichloromethane (with a dielectric constant of 9.08) in the geometric optimization.

**Photophysical Experiments.** Absorption spectra were recorded using a Shimadzu 2445 UV/vis spectrophotometer using 1 cm path-length quartz cuvettes. The steady-state emission spectra were measured using a PTI QM-4CW system, and an excitation source with the spectral bandpass of 2 nm was used. Quantum yields were measured using comparative method at room temperature in a dichloromethane solution. The solution was deoxygenated by purging with argon gas for 20 min. A long-necked 1 cm quartz cuvette was used for measurements. The cuvette was cooled with a dry ice-acetone bath to prevent solvent loss. The optical density of both sample and reference solutions was maintained below 0.1 AU at and above the excitation wavelength. A solution of quinine sulfate[27] dihydrate in 0.1 N $H_2SO_4$ was used as a reference. Emission spectra in a frozen glass were recorded in 2-MeTHF at 77 K. Solid state emission spectra were recorded at room temperature using a powder sample holder. Phosphorescence lifetime measurements were performed on the same fluorimeter equipped with variable high rep rate pulsed xenon source for excitation and were limited to lifetimes >0.4 $\mu$s. Delayed phosphorescent emission spectra of the ligands were measured using a gated analog detector with R928 red extended PMT in 2-MeTHF at 77 K.

**X-ray Crystallography.** *Data Collection and Processing.* The crystals were prepared using the solvent diffusion method. The sample was mounted on a Mitegen polyimide micromount with a small amount of Paratone N oil. All X-ray measurements were made on a Bruker-Nonius Kappa Axis X8 Apex2 diffractometer at a temperature of 110 K. The data collection strategy was a number of $\omega$ and $\varphi$ scans. The frame integration was performed using SAINT.[28] The resulting raw data was scaled and absorption corrected using a multiscan averaging of symmetry equivalent data using SADABS[29] for **1a**, **1b**, and **3a** and using TWINABS[30] for **2b** and **3b**. The structure was solved by direct methods using the XS program[31] except for **2b** for which the SIR92 program[32] was used. All non-hydrogen atoms were obtained from the initial solution. The hydrogen atoms were introduced at idealized positions and were allowed to ride on the parent atom. The structural model was fit to the data using full matrix least-squares based on $F^2$. The calculated structure factors included corrections for anomalous dispersion from the usual tabulation. The structure was refined using the XL program from SHELXTL,[33] and graphic plots were produced using the NRCVAX crystallographic program suite.

## ■ ASSOCIATED CONTENT

### Ⓢ Supporting Information

Crystallographic data (CIF) for **1a**, **1b**·$CH_2Cl_2$, **2b**, **3a**, and **3b**. Crystal data and refinement details for **1a**, **1b**·$CH_2Cl_2$, **2b**, **3a**, and **3b**. Electronic spectra of the ligands. Solvent effects. Stern−Volmer plots for **2b** and **3b**. DFT calculation results. This material is available free of charge via the Internet at http://pubs.acs.org.

## ■ AUTHOR INFORMATION


### Corresponding Author

*E-mail: huos@ecu.edu.

### Present Addresses

[§]Department of Chemistry, Georgia Institute of Technology, Atlanta, GA 30332.

[∥]Department of Chemistry, Western University, London, ON N6A 5B7. Canada.


### Notes

The authors declare no competing financial interest.

## ■ ACKNOWLEDGMENTS

S.H. acknowledges financial support from the Research Corporation for Science Advancement through a Cottrell College Science Award. P.D.B. thanks the Department of Chemistry of North Carolina State University and the State of North Carolina for funding the purchase of the Apex2 diffractometer.

## ■ REFERENCES


(1) (a) Ma, Y.-G.; Cheung, T.-C.; Che, C.-M.; Shen, J.-C. *Thin Solid Films* **1998**, *333*, 224−227. (b) Evans, R. C.; Douglas, P.; Williams, J. A. G.; Rochester, D. L. *J. Fluorescence* **2006**, *16*, 201−206. (c) Thomas, S. W., III; Venkatesan, K.; Muller, P.; Swager, T. M. *J. Am. Chem. Soc.* **2006**, *128*, 16641−16648. (d) Siu, P. K.-M.; Lai, S.-W.; Lu, W.; Zhu, N.; Che, C.-M. *Eur. J. Inorg. Chem.* **2003**, 2749−2752. (e) Lanoë, P.-H.; Fillaut, J.-L.; Toupet, L.; Williams, J. A. G.; Bozec, H. L.; Guerchais, V. *Chem. Commun.* **2008**, 4333−4335. (f) Wong, K.-H.; Chan, M. C.-W.; Che, C.-M. *Chem.—Eur. J.* **1999**, *5*, 2845−2849. (g) Koo, C.-K.; Ho, Y.-M.; Chow, C.-F.; Lam, M. H.-W.; Lau, T.-C.; Wong, W.-Y. *Inorg. Chem.* **2007**, *46*, 3603−3612.

(2) (a) Siu, P. K.-M.; Ma, D.-L.; Che, C.-M. *Chem. Commun.* **2005**, 1025−1027. (b) Botchway, S. W.; Charnley, M.; Haycock, J. W.; Parker, A. W.; Rochester, D. L.; Weinstein, J. A.; Williams, J. A. G. *Proc. Natl. Acad. Sci. U.S.A.* **2008**, *105*, 16071−16076. (c) Ma, D.-L.; Che, C.-M.; Yan, S.-C. *J. Am. Chem. Soc.* **2009**, *131*, 1835−1846. (d) Wu, P.; Wong, E.L.-M.; Ma, D.-L.; Tong, G. S.-M.; Ng, K.-M.; Che, C.-M. *Chem.—Eur. J.* **2009**, *15*, 3652−3656. (e) Baggaley, E.; Weinstein, J. A.; Williams, J. A. G. *Coord. Chem. Rev.* **2012**, *256*, 1762−1785.

(3) For recent reviews on OLED applications of platinum complexes, see: (a) Williams, J. A. G.; Develay, S. D.; Rochester, D. L.; Murhy, L. *Coord. Chem. Rev.* **2008**, *252*, 2596−2611. (b) Xiang, H.-F.; Lai, S.-W.; Lai, P. T.; Che, C.-M. Phosphorescent platinum(II) materials for OLED applications. In *Highly Efficient OLEDs with Phosphorescent Materials*; Yersin, H., Ed.; Wiley-VCH: Weinheim, 2008. (c) Kalinowski, J.; Fattori, V.; Cocchi, M.; Williams, J. A. G. *Coord. Chem. Rev.* **2011**, *255*, 2401−2425.
(4) Ravindranathan, D.; Vezzu, D. A. K.; Bartolotti, L.; Boyle, P. D.; Huo, S. *Inorg. Chem.* **2010**, *49*, 8922−8928.
(5) Vezzu, D. A. K.; Ravindranathan, D.; Garner, A. W.; Bartolotti, L.; Smith, M. E.; Boyle, P. D.; Huo, S. *Inorg. Chem.* **2011**, *50*, 8261−8273.
(6) Vezzu, D. A. K.; Deaton, J. C.; Jones, J. S.; Bartolotti, L.; Harris, C. F.; Marchetti, A. P.; Kondakova, M.; Pike, R. D.; Huo, S. *Inorg. Chem.* **2010**, *49*, 5107−5119.
(7) Huo, S.; Harris, C. F.; Vezzu, D. A. K.; Gagnier, J.; Smith, M. E.; Pike, R.; Li, Y. *Polyhedron* **2013**, *52*, 1030−1040.
(8) (a) Li, K.; Guan, X.; Ma, C.-W.; Lu, W.; Chen, Y.; Che, C.-M. *Chem. Commun.* **2011**, *47*, 9075−9077. (b) Kui, S. C. F.; Chow, P. K.; Tong, G. S. M.; Lai, S.-L; Cheng, G.; Kwok, C.-C.; Low, K.-H; Ko, M.-Y.; Che, C.-M. *Chem.—Eur. J.* **2013**, *19*, 69−73. (c) Kui, S. C. F.; Chow, P. K.; Chang, G.; Kwok, C.-C.; Kwong, C. L.; Low, K.-H.; Che, C.-M. *Chem. Commun.* **2013**, *49*, 1497−1499.
(9) (a) Williams, J. A. G.; Beeby, A.; Davies, E. S.; Weinstein, J. A.; Wilson, C. *Inorg. Chem.* **2003**, *42*, 8609−8611. (b) Farley, S. J.; Rochester, D. L.; Thompson, A. L.; Howard, J. A. K.; Williams, J. A. G. *Inorg. Chem.* **2005**, *44*, 9690−9703. (c) Develay, S.; Blackburn, O.; Thompson, A. L.; Williams, J. A. G. *Inorg. Chem.* **2008**, *47*, 11129−11142. (d) Rochester, D. L.; Develay, S.; Záliš, S.; Williams, J. A. G. *Dalton Trans.* **2009**, 1728−1714. (e) Wang, Z.; Turner, E.; Mahoney, V.; Madakuni, S.; Groy, T.; Li, J. *Inorg. Chem.* **2010**, *49*, 11276−11286.
(10) (a) Constable, E. C.; Henney, R. P. G.; Leese, T. A.; Tocher, D. A. *J. Chem. Soc., Chem., Commun.* **1990**, 513−515. (b) Cheung, T.-C.; Cheung, K.-K.; Peng, S.-M.; Che, C.-M. *J. Chem. Soc., Chem. Dalton Trans.* **1996**, 1645. (c) Neve, F.; Crispini, A.; Campagna, S. *Inorg. Chem.* **1997**, *36*, 6150−6156. (c) Lai, S.-W.; Chan, M. C. W.; Cheung, T.-C.; Peng, S.-M.; Che, C.-M. *Inorg. Chem.* **1999**, *38*, 4046−4055. (d) Hofmann, A.; Dahlenburg, L.; van Eldik, R. *Inorg. Chem.* **2003**, *42*, 6528−6538.
(11) (a) Garner, K. L.; Parkes, L. F.; Piper, J. D.; Williams, J. A. G. *Inorg. Chem.* **2010**, *49*, 476−487. For other related six−six-membered metallacycles, see (b) Song, D.; Wu, Q.; Hook, A.; Kozin, I.; Wang, S. *Organometallics* **2001**, *20*, 4683−4689. (c) Abrahamsson, M.; Jäger, M.; Kumar, R. J.; Österman, T.; Eriksson, L.; Persson, P.; Becker, H.-C.; Johansson, O.; Hammarström, L. *J. Am. Chem. Soc.* **2006**, *128*, 12616−12617. (d) Abrahamsson, M.; Jäger, M.; Kumar, R. J.; Österman, T.; Persson, P.; Becker, H.-C.; Johansson, O.; Hammarström, L. *J. Am. Chem. Soc.* **2008**, *130*, 15533−15542.
(12) Yang, J.-S.; Lin, Y.-H.; Yang, C.-S. *Org. Lett.* **2002**, *4*, 777−780.
(13) Antilla, J. C.; Klapars, A.; Buchwald, S. L. *J. Am. Chem. Soc.* **2002**, *124*, 11684−11688.
(14) Garner, A. W.; Harris, C. F.; Vezzu, D. A. K.; Pike, R. D.; Huo, S. *Chem. Commun.* **2011**, *47*, 1902−1904.
(15) Sajith, P. K.; Suresh, C. H. *Dalton Trans.* **2010**, *39*, 815−822.
(16) (a) Chan, C.-W.; Cheng, L.-K.; Che, C.-M. *Coord. Chem. Rev.* **1994**, *132*, 87−97. (b) Yam, V. W.-W.; Wong, K. M.-C. *Top. Curr. Chem.* **2005**, *257*, 1−32. (c) Castellano, F. N.; Pomestchenko, I. E.; Shikhova, E.; Hua, F.; Muro, M. L.; Rajapakse, N. *Coord. Chem. Rev.* **2006**, *250*, 1819−1828. (d) Wong, K. M.-C.; Yam, V. W.-W. *Coord. Chem. Rev.* **2007**, *251*, 2477−2488.
(17) (a) Lu, W.; Mi, B.-X.; Chan, M. C. W.; Hui, Z.; Che, C.-M.; Zhu, N.; Lee, S. T. *J. Am. Chem. Soc.* **2004**, *126*, 4958−4971. (b) Schneider, J.; Du, P.; Wang, X.; Brennessel, W. W.; Eisenberg, R. *Inorg. Chem.* **2009**, *48*, 1498−1506. (c) Schneider, J.; Du, P.; Jarosz, P.; Lazarides, T.; Wang, X.; Brennessel, W. W.; Eisenberg, R. *Inorg. Chem.* **2009**, *48*, 4306−4316.
(18) Kui, S. C.; Sham, I. H. T.; Cheung, C. C. C.; Ma, C.-W.; Yan, B.; Zhu, N.; Che, C.-M.; Fu, W.-F. *Chem.—Eur. J.* **2007**, *13*, 417−435.
(19) Tong, G.-M.; Che, C.-M. *Chem.—Eur. J.* **2009**, *15*, 7225−7237.
(20) (a) Connick, W. B.; Gray, H. B. *J. Am. Chem. Soc.* **1997**, *119*, 11620−11627. (b) Connick, W. B.; Geiger, D.; Eisenberg, R. *Inorg. Chem.* **1999**, *38*, 3264−3265.
(21) Leung, S. Y.-L.; Lam, E. S.-H.; Lam, W. H.; Wong, K. M.-C.; Wong, W.-T.; Yam, V. W.-W. *Chem.—Eur. J.* **2013**, *19*, 10360−10369.
(22) (a) Delley, B. *J. Chem. Phys.* **1990**, *92*, 508−517. (b) Delley, B. *J. Chem. Phys.* **2000**, *113*, 7756−7764. We chose to use DeMol3 to optimize the geometries because it is faster than G09, and we also found that DeMol3 produces geometries very close to those revealed by the X-ray crystallography. As DeMol3 does not contain the program for TDDFT calculations, the performance of TDDFT calculations, as suggested by a reviewer, was not made.
(23) Tsuneda, T.; Suzumura, T.; Hirao, K. *J. Chem. Phys.* **1999**, *110*, 10664−10678.
(24) Delley, B. *Int. J. Quantum Chem.* **1998**, *69*, 423−433.
(25) Peterson, K. A.; Figgen, D.; Goll, E.; Stoll, H.; Dolg, M. *J. Chem. Phys.* **2003**, *119*, 11113−11123.
(26) Klamt, A.; Schuurmann, G. *J. Chem. Soc., Perkin Trans. 2* **1993**, 799−805.
(27) Meech, S. R.; Phillips, D. *J. Photochem.* **1983**, *23*, 193−217.
(28) Bruker-Nonius, SAINT version 2009.9, 2009, Bruker-Nonius, Madison, WI.
(29) Bruker-Nonius, SADABS version 2009.9, 2009, Bruker-Nonius, Madison, WI.
(30) Bruker-Nonius, TWINABS version 2009.9, 2009, Bruker-Nonius, Madison, WI.
(31) Bruker-AXS, XS version 2009.9, 2009, Bruker-AXS, Madison, WI.
(32) Altomare, A.; Cascarano, G.; Giacovazzo, C.; Guagliardi, A.; Burla, M. C.; Polidori, G.; Camalli, M. *J. Appl. Crystallogr.* **1994**, *27*, 435.
(33) Bruker-AXS, XL version 2009.9, 2009, Bruker-AXS, Madison, WI.